Journal of Catalysis 276 (2010) 123–133

Contents lists available at ScienceDirect

Journal of Catalysis

journal homepage: www.elsevier.com/locate/jcat

Three-dimensional cubic mesoporous materials with a built-in N-heterocyclic carbene for Suzuki–Miyaura coupling of aryl chlorides and C(sp^3)-chlorides

Hengquan Yang [a,*], Guang Li [a], Zhancheng Ma [a], Jianbin Chao [b], Zhiqiang Guo [b]

[a] School of Chemistry and Chemical Engineering, Shanxi University, Taiyuan 030006, PR China
[b] The Institute of Applied Chemistry, Shanxi University, Taiyuan 030006, PR China

ARTICLE INFO

Article history:
Received 10 May 2010
Revised 27 August 2010
Accepted 4 September 2010
Available online 8 October 2010

Keywords:
Mesoporous material
N-heterocyclic carbene
Suzuki–Miyaura coupling
Aryl chloride
SBA-16

ABSTRACT

New cubic cage-like mesoporous materials with a bulky N-heterocyclic carbene [IPr, 1,3-bis(2,6-diisopropylphenyl)imidazol-2-ylidene] precursor in the framework were synthesized by a co-condensation of IPr precursor-bridged organosilane and TEOS in the presence of template. N_2 sorption, XRD and TEM characterizations revealed that the mesostructural orderings of the synthesized materials depended on the molar fraction of the bridged organosilane in the initial gel mixture. With the increase in the molar fraction of the organosilane from 2.5% to 15%, the mesostructure of the synthesized material changed from a well-ordered 3D ordered structure to a amorphous structure. FT-IR and solid-state NMR characterizations confirmed that IPr carbene precursor was covalently integrated with the solid materials. Such hybrid materials were able to coordinate $Pd(acac)_2$, leading to active solid catalysts for Suzuki–Miyaura couplings of less reactive aryl chlorides. The solid catalyst could be reused 8 times without a significant decrease in activity. Furthermore, the solid catalyst was active for the coupling of C(sp^3)-chlorides and arylboronic acids.

1. Introduction

The Pd-catalyzed Suzuki–Miyaura coupling is currently a fundamental reaction for the synthesis of polymers, agrochemical and pharmaceutical compounds [1–3]. The use of aryl chlorides as substrates has proven difficult but is highly desirable in view of the wide diversity, ready availability and low cost of aryl chlorides in contrast with aryl bromides and iodides. N-heterocyclic carbene complex Pd–IPr [IPr = N,N′-bis(2,6-diisopropylphenyl)imidazol-2-ylidene] was recently found to be the most efficient catalyst for Suzuki–Miyaura coupling of aryl chlorides [4–10]. Compared with the well-established phosphine systems, Pd–IPr complex is more appealing because it is air-stable and low toxic. Such advantages make Pd–IPr complex a potential catalyst for practical applications if this complex can be immobilized in a proper fashion for easy reuse. However, there is no report on immobilization of the bulky bis(2,6-diisopropylphenyl)-substituted carbene Pd complex for Suzuki–Miyaura coupling although the grafting of small methyl-substituted carbene complexes on insoluble supports has been reported [11,12], which exhibited low activity toward aryl chlorides due to lacking bulky electron-donating groups like 2,6-diisopropylphenyl group on the imidazole ring [13–19].

Recently, a new concept for preparing solid catalysts has been developed with the discovery of hybrid periodic mesoporous materials. Such materials can be prepared by co-condensation of complex/ligand-bridged trialkoxysilane and tetraalkoxysilane in the presence of template (namely, a mixture of complex/ligand-bridged trialkoxysilane and tetraalkoxysilane was hydrolyzed and condensed in an aqueous medium at a molecular level in one pot) [20–27]. This method opens a promising avenue for creating hybrid solid catalysts with open and ordered mesostructures which facilitate the accessibility of active sites. Compared to the widely used grafting method [20,28], it endows the solid catalyst with larger surface area and higher pore volume owing to the incorporation of organic moieties in the framework instead of grafting on the surface. Moreover, the co-condensation method leads to a more homogeneous distribution of active sites throughout the solid materials and a larger degree of immobilization because the hydrolysis–condensation of siliceous precursors usually occurs under strong basic or acidic aqueous conditions that enable the trialkoxysilyl groups to completely hydrolyze and further condense into Si—O—Si linkages [29].

Driven by such advantages, Dufaud et al. synthesized a periodic mesoporous hybrid material containing a rhodium organophosphine complex in the framework [30]. This hybrid material showed high activity and good recyclability in the hydrogenation of alkenes. Corma's group synthesized periodic mesoporous hybrid materials with a vanadyl Schiff base and a carbapalladacycle

* Corresponding author. Fax: +86 351 7011688.
E-mail address: hqyang@sxu.edu.cn (H. Yang).

0021-9517/$ - see front matter © 2010 Elsevier Inc. All rights reserved.
doi:10.1016/j.jcat.2010.09.004

complex in the frameworks [29,31]. These materials were catalytically active toward the cyanosilylation of benzaldehyde and Suzuki–Miyaura coupling of aryl bromides. Yang's group has recently prepared hybrid mesoporous materials with a built-in chiral diaminocyclohexane and BINAP, which exhibit good to excellent performances in the asymmetric hydrogenation of ketones [25,32].

However, in contrast to the ever-expanding families of metal complex catalysts, the catalytically active hybrid mesoporous materials prepared with this elegant method are rather limited. Moreover, the reported, catalytically active hybrid mesoporous materials are limited to two-dimensional (2D) channel-like hexagonal (p6 mm) materials such as MCM-41 and SBA-15 [33,34]. Compared with 2D channel-like hexagonal mesoporous material, the three-dimensional (3D) cubic mesostructure of SBA-16 (*Im3m*, body-centered cubic) was found to be more attractive due to the 3D cage-like mesoporous network (in which each spherical cage is connected with eight neighboring cages through entrances) [35–38]. Such a unique mesostructure of SBA-16 was proven to facilitate the fast diffusions of reaction molecules [39–41]. However, up to date, there is still no report on the catalytically active SBA-16 type of hybrid materials synthesized through the co-condensation of the bridged organosilane.

Herein, we report the successful synthesis of a new type of 3D cubic mesoporous hybrid materials containing IPr precursor in the framework. By the coordination of the synthesized hybrid material with $Pd(acac)_2$, a novel heterogeneous hybrid catalyst has been derived, which is active and recyclable for Suzuki–Miyaura couplings of aryl chlorides and $C(sp^3)$-chlorides.

2. Experimental

2.1. Reagents and materials

Pluronic P123 ($EO_{20}PO_{70}EO_{20}$) and F127 ($EO_{106}PO_{70}EO_{106}$) were purchased from Sigma Company. $Pd(acac)_2$ (acac = acetylacetonate) was obtained from Kaida Metal Catalyst & Compounds Co. Ltd. (China). Various arylboronic acids were obtained from Beijing Pure Chemical Co. Ltd. Aryl chlorides, ICl and bromides were purchased from Aladdin Company. 2,6-Diisopropylaniline and other reagents were obtained from Shanghai Chemical Reagent Company of Chinese Medicine Group. All solvents were of analytical quality.

2.2. Synthesis of 4-iodo-2,6-diisopropylaniline (*1*)

The route for the synthesis of the IPr precursor-bridged organosilane is described in Scheme 1. 2,6-Diisopropylaniline (13.19 g) was dissolved in a mixture of methanol and dichloromethane (135 mL, 1:1). Iodochloride (12.1 g) dissolved in a mixture of methanol–dichloromethane (15 mL, 1:1) was added into the solution of 2,6-diisopropylaniline [34]. The resultant mixture was stirred at room temperature for 24 h and then at 40 °C for 16 h. At the end of the reaction, the solvent was evaporated out. The resultant crude solid product was treated with 40 mL of an aqueous sodium hydroxide solution (20 wt%) and then extracted with diethyl ether (3 × 35 mL). After drying over sodium sulfate, the solvent was evaporated out. Compound **1** was eventually obtained after distillation under reduced pressure (12.2 g, yield = 54.4%). ^1H NMR ($CDCl_3$): 7.19 (s, 2 H); 3.43 (s, 2 H); 2.77–2.84 (m, 2H), 1.20 (s, 12).

2.3. Synthesis of bis(4-iodo-2,6-diisopropylphenyl)diazabutadiene (*2*)

Glyoxal (3.6 g; 40 wt% in water) was added dropwise into 126 mL of methanol containing 15.1 g of 4-iodo-2,6-diisopropylaniline. Seventeen drops of formic acid were also added into this system as catalyst. The reaction mixture was stirred at room temperature for 16 h and at 40 °C for another 24 h. The yellow solid was achieved by a filtration and washed with methanol, leading to the title compound **2** (yield = 70.0%). ^1H NMR ($CDCl_3$): 8.01 (s, 2 H); 7.34–7.44 (m, 4 H); 2.79–2.84 (m, 4 H); 1.02–1.17 (m, 24 H).

2.4. Synthesis of 1,3-bis(4-iodo-2,6-diisopropylphenyl)-1H-imidazol-3-ium trifluoromethane-sulfonate (*3*)

Compound **2** (3.15 g) was dissolved in 39 mL of dry dichloromethane. Chloromethyl pivalate (1.25 g) and silver trifluoromethane sulfonate (1.67 g) were added into this dichloromethane solution. The reaction mixture was heated to reflux for 25 h. After cooling to room temperature, the formed precipitate (silver chloride) was removed by filtration. The solution was concentrated, giving the crude product. The pure compound **3** was obtained after recrystallization in a mixture of methanol and diethyl ether (yield = 65.0%). ^1H NMR ($CDCl_3$): 10.1 (s, 1 H); 8.51 (s, 2 H); 7.84 (s, 4 H); 2.20–2.23 (m, 4 H); 1.09–1.22 (m, 24 H).

2.5. Synthesis of 1,3-bis(4-triethoxysilyl-2,6-diisopropylphenyl l)-1H-imidazol-3-ium trifluoromethane-sulfonate (*4*)

Compound **3** (2.7 g), $Rh(cod)(CH_3CN)_2BF_4$ (0.075 g), triethoxysilane (5.5 g) and triethylamine (4.3 g) were dissolved in 60 mL of dry DMF. The resulting solution was stirred at 80 °C for 8 h under N_2 atmosphere. After cooling, the solvent was removed off by distillation, and the resultant brown residue was dissolved in 60 mL of dichloromethane (DCM). After removal of the precipitation by filtration, the DCM solution was washed with cold water

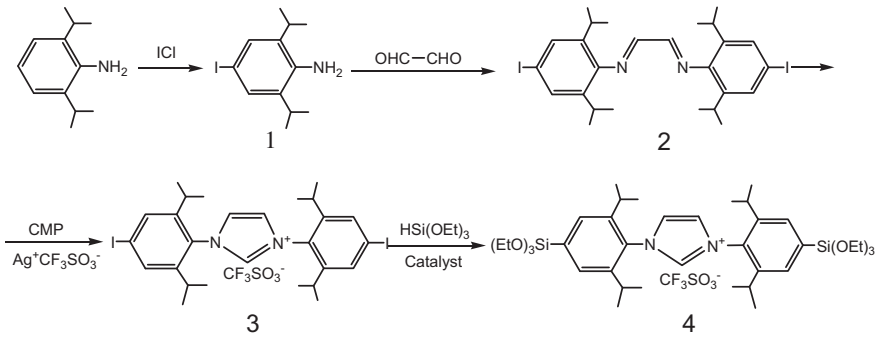

CMP = chloromethyl pivalate; Catalyst = $Rh(cod)(CH_3CN)_2\,BF_4$

Scheme 1. Synthesis routes for IPr precursor-bridged triethoxysilane [IPr, 1,3-bis(2,6-diisopropylphenyl) imidazol-2-ylidene].

(5 × 30 mL). The organic phase was dried over sodium sulfate and filtered. After concentration, compound **4** was achieved (yield = *ca.* 80%). ^{1}H NMR ($CDCl_3$): 10.18 (s, 1 H); 8.54 (s, 2 H); 7.52–7.64 (m, 4 H); 3.68–3.95 (m, 12 H); 2.43 (m, 4 H); 1.25–1.32 (m, 42 H). ^{13}C NMR (DMSO) is shown in Section 3.

2.6. Synthesis of the hybrid mesoporous materials

The cubic mesoporous materials containing IPr (Scheme 2) were synthesized by the condensation of compound **4** and tetraethyl orthosilicate (TEOS) in the presence of a mixture of P123 and F127 as template. A mixture of F127 (0.62 g) and P123 (0.1 g) was dissolved in a solution of 25 g of distilled water and 5 g of concentrated hydrochloric acid (36.5%). After the solution was stirred at 35 °C for 5 h, total 10.5 mmol of the total siliceous precursors dissolved in 3 mL of ethanol was added dropwise to the above solution. The molar fraction of **4** [$2M_4/(2M_4 + MTEOS)$, wherein M is the molar numbers] in the total siliceous precursors was tuned from 2.5% to 5%, 7.5%, 10%, 12.5% and 15%. After stirring for 40 min, the resultant suspension was transferred into autoclaves and treated at 35 °C for 24 h under static conditions. Afterward, the temperature was raised up to 100 °C and the suspension was kept at this temperature for 24 h. After the hydrothermal process, the precipitated solid was isolated by filtration, washed with water and ethanol, and then dried at room temperature for 12 h. The template was removed by repeated extractions with a diluted ethanolic HCl solution under the refluxing conditions (1 g of the hybrid material, 0.5 g of concentrated HCl solution and 50 mL of ethanol). According to the molar fraction of compound **4** in the total silicon precursors, six materials, SBA-16-IPr(2.5%), SBA-16-IPr(5%), SBA-16-IPr(7.5%), SBA-16-IPr(10%), SBA-16-IPr(12.5%) and SBA-16-IPr(15%), were obtained (the number in parentheses means the molar percent of compound **4** in the total silicon precursor).

2.7. Coordination of SBA-16-IPr(χ) materials with Pd(acac)$_2$

SBA-16-IPr(χ) (1.0 g; dried at 100 °C for 4 h) was dispersed in 30 mL of dry 1,4-dioxane containing 0.02 g of $Pd(acac)_2$ (acac = acetylacetonate). After the mixed system was stirred at 100 °C for 40 h under N_2 atmosphere, 1,4-dioxane was removed by filtration, affording a brown solid. The solid was repeatedly washed with dry 1,4-dioxane and dried under vacuum. The eventually achieved solid was designated as SBA-16-IPr(χ)–Pd. The homogeneous catalyst was prepared through the coordination of **4** with $Pd(acac)_2$ (the molar ratio is 1:1) for comparison.

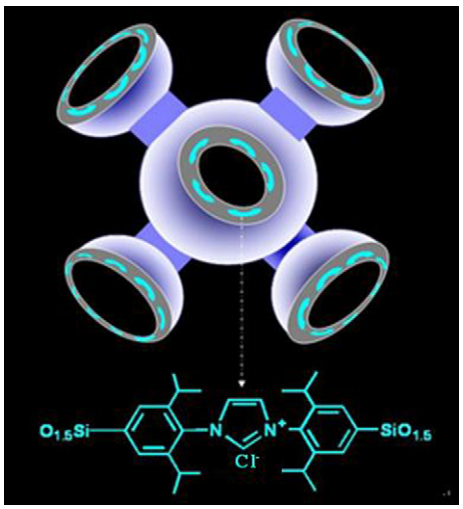

Scheme 2. The structural model for the hybrid mesoporous materials SBA-16-IPr(χ). Note: for clarification, another four entrances are omitted. In fact, each spherical cage is connected with eight neighboring cages through entrances.

2.8. General procedure for Suzuki–Miyaura coupling of aryl chlorides and arylboronic acids

A mixture of aryl chlorides (2 mmol), phenylboronic acid (2.2 mmol), potassium *tert*-butoxide (3 mmol), *iso*-propyl alcohol (6 mL) and the catalyst SBA-16-IPr(χ)–Pd was stirred at 80 °C under N_2 atmosphere for a given time. At the end of the reaction, the mixture was cooled down to room temperature and repeatedly extracted with diethyl ether. The combined organic layers were concentrated, and the resulting product was purified by column chromatography on silica gel. The products were confirmed by ^{1}H NMR (Supplementary material). The purity was confirmed by GC.

The recycling test for the Suzuki–Miyaura coupling was conducted as follows: for the first run, a mixture of 12 mmol of 4′-chloroacetophenone, 13.2 mmol of phenylboronic acid, 18 mmol of potassium *tert*-butoxide, SBA-16-IPr(10%)–Pd (0.5 mol% Pd with respect to aryl chloride), 36 mL of *iso*-propyl alcohol was stirred at 80 °C under N_2 atmosphere. At the end of the reaction, the system was cooled down to room temperature and repeatedly extracted with diethyl ether. The recovered catalyst was washed with diethyl ether, water, methanol and acetone in sequence and then dried under vacuum. The recovered catalyst was weighed again. The fresh solvent and substrate were added, but the molar ratio of substrate to Pd remained the same as that in the first run.

2.9. General procedure for the coupling reactions of benzylic/allylic chlorides and arylboronic acids

A mixture of benzylic or allylic chlorides (2 mmol), phenylboronic acid (2.2 mmol), potassium *tert*-butoxide (3 mmol), *iso*-propyl alcohol (6 mL), and the catalyst SBA-16-IPr(10%)–Pd was stirred at 80 or 50 °C under N_2 atmosphere. At the end of reaction, the mixture was cooled down to room temperature and repeatedly extracted with diethyl ether. The combined organic layers were concentrated, and the resulting product was purified by a column chromatography on silica gel. The products were confirmed by ^{1}H NMR (Supplementary material).

2.10. Characterization and analysis

Small-angle powder X-ray powder diffraction was performed on Rigaku (Cu Ka, 40 kV, 30 mA). N_2 physical adsorption was carried out on a micrometrics ASAP2020 volumetric adsorption analyzer (before measurements, samples were out gassed at 125 °C for 6 h). The Brunauer–Emmett–Teller (BET) surface area was evaluated from data in the relative pressure range of 0.05–0.15. The total pore volume of each sample was estimated from the amount adsorbed at the highest P/P_0 (above 0.99). Pore diameters were determined from the adsorption branch using the Barrett–Joyner–Halenda (BJH) method. FT-IR spectra were collected on a PE-1730 infrared spectrometer. Pd content was analyzed with an inductively coupled plasma-atomic emission spectrometry (ICP-AES, AtomScan16, TJA Co.). C and N content analysis was conducted on Vario EL (Elementar). X-ray photoelectron spectra (XPS) were recorded on a Kratos Axis Ultra DLD, and the C_{1S} line at 284.8 eV was used as a reference. TEM micrographs were taken with a JEM-2000EX transmission electron microscope at 120 kV. Solid-state NMR spectra were recorded on an Infinityplus 300 MHz spectrometer: for ^{13}C CP-MAS NMR experiments, 75.4 MHz resonant frequency, 4 kHz spin rate, 4 s pulse delay,

1.0 ms contact time, hexamethyl benzene as a reference compound; for ^{13}Si CP-MAS NMR experiments, 79.6 MHz resonant frequency, 4 kHz spin rate, 4.0 s pulse delay, TMS as a reference compound. GC analysis was conducted on a SP-GC6800A.

3. Results and discussion

3.1. Synthesis of IPr precursor-bridged organosilane and the hybrid materials

In order to incorporate IPr into a material framework through a hydrolysis–condensation process, we need to derive IPr carbene precursor with hydrolyzable alkoxysilyl groups. Here, we followed a modified route for the introduction of two trialkoxysilyl groups to the terminals of IPr precursor (Scheme 1, compound **4**) [34]. At first, iodination of 2,6-diisopropylaniline with iodine chloride gave 4-iodo-2,6-dimethylaniline (compound **1**). In the second step, compound **1** was reacted with glyoxal, leading to a bis-Schiff's base compound **2**. Compound **2** was then subjected to a ring-closing step in the presence of silver salt, yielding an iodo-substituted IPr precursor (compound **3**). This compound was then silylated with $HSi(OEt)_3$ using a Rh complex as catalyst, eventually affording IPr precursor-bridged organosilane (compound **4**, confirmed by ^{1}H NMR and ^{13}C NMR). The whole process included four steps, and the yields for every step were over 50%.

The hybrid materials were fabricated via a modified procedure for synthesizing SBA-16 [36]. Because compound **4** has a bulky organic group between two triethoxysilyl groups, it is necessary to use other small silane compounds such as TEOS to co-condense with **4** for constructing an ordered mesostructure. Previous studies revealed that the presence of bulky group-bridged organosilane usually influenced the mesostructural ordering and even induced the mesophase changes [42]. With these considerations, the molar fraction of **4** in the initial total siliceous precursors [$(2M_4/(2M_4 + M_{TEOS})$, wherein M is the molar numbers], was finely tuned from 2.5% to 5%, 7.5%, 10%, 12.5% and 15%. Block copolymer F127 admixed with a little amount of block copolymer P123 was chosen as template because the presence of P123 was favorable to tune the textural properties. Compound **4** does not dissolve in TEOS. So, a series of organic solvents were preliminarily screened to find one which can assist the dissolution of **4** in TEOS. Ethanol was found to be a good solvent. Under our synthesis conditions, 3 mL of ethanol was essential to dissolve **4** and achieve hybrid mesoporous materials with a homogeneous appearance. The lack of ethanol led to a solid material with an unevenly distributed color, suggesting that a phase separation occurred during the synthesis. The excess of ethanol probably caused a deterioration of the mesostructural ordering. After the hydrothermal synthesis, the template filled in the pores was repeatedly extracted by refluxing in an acidic ethanol solution. Eventually, six SBA-16-IPr(χ) materials were obtained (Scheme 2), wherein χ equals to 2.5%, 5%, 7.5%, 10%, 12.5% or 15% according to the molar fraction of **4** in the initial gel mixture.

3.2. Structural characterization

In order to investigate the effects of the contents of **4** on the structure and physical properties of the obtained hybrid materials, N_2 sorption, XRD and TEM were employed to characterize SBA-16-IPr(χ) materials.

The N_2 sorption isotherms of SBA-16-IPr(χ) samples are presented in Fig. S1 (Supplementary material). The corresponding pore size distribution curves are displayed in Fig. S2 (Supplementary material).Their textural parameters measured with N_2 sorption are summarized in Table 1. SBA-16-IPr(2.5%) shows a type IV isotherm with a steep capillary condensation/evaporation step and a type H2 hysteresis loop at the relative pressure of 0.45–0.7, which is characteristic of a high-quality cage-like pore structure of a typical SBA-16. The pore size plot calculated from N_2 adsorption branch exhibits a narrow distribution centered at 5.5 nm. The specific surface area and pore volume of SBA-16-IPr(2.5%) are 753 m^2/g and 0.65 cm^3/g, respectively (in Table 1), which fall in the ranges of a typical cubic mesoporous material. The hysteresis loop shows a slight shift to the lower relative pressure when the molar fraction of **4** in the initial gel mixture increases up to 5%. This is an indication of a decrease in the pore size (down to 5.3 nm, in Table 1). As the molar fraction of **4** in the initial gel mixture further increases up to 7.5% and 10%, the textural parameters such as pore size, specific surface area and pore volume continue decreasing (Table 1). This trend probably reflects the changes in the interactions between the silicon species and template molecules. Till the molar fraction of **4** increases up to 12.5%, the nitrogen adsorption/desorption isotherm remains a type IV of a cage-like mesoporous structure. However, the molar fraction up to 15% led to considerable changes in the isotherm. The isotherm shows two steps of less steep capillary condensation/evaporation, indicating a nonuniform distribution of pore sizes.

Table 1
Physical parameters of SBA-16-IPr(χ) materials.

Samples	S[a] (m^2/g)	P[b] (cm^3/g)	D[c] (nm)	C(·)[d] (wt%)	N(·)[d] (wt%)
SBA-16-IPr(2.5%)	753	0.65	5.5	8.3 (6.3)	0.5 (0.5)
SBA-16-IPr(5%)	703	0.63	5.3	14.8 (12.0)	0.9 (1.0)
SBA-16-IPr(7.5%)	670	0.58	4.7	20.2 (17.0)	1.3 (1.5)
SBA-16-IPr(10%)	645	0.55	4.6	24.3 (21.5)	1.8 (2.1)
SBA-16-IPr(12.5%)	752	0.62	4.2	–	–
SBA-16-IPr(15%)	576	0.58	4.0 (14.0)[e]	–	–

[a] BET surface area.
[b] Single-point pore volume calculated at a relative pressure P/P_0 of 0.99.
[c] BJH method from adsorption branch.
[d] Determined by combustion chemical analysis; the data in parentheses are the theoretical values.
[e] The data in parentheses are the second pore diameter.

The XRD patterns of SBA-16-IPr(χ) materials are displayed in Fig. S3 (Supplementary material). For the sample SBA-16-IPr(2.5%), the XRD pattern shows a strong peak at $2\theta = 0.85°$, which is attributed to the (1 1 0) reflection. Two small peaks at $2\theta = 1.12°$ and $2\theta = 1.77°$ can be also observed (inset in Fig. S3, Supplementary material), which are assigned to the (2 0 0) and (3 1 1) reflections, respectively. Such assignments for these three diffraction peaks are in consistent with a cubic *Im3m* symmetry. When the molar fraction of **4** increases up to 5%, the peaks of the (1 1 0) reflections along with the (2 0 0) and (3 1 1) reflections can be still observed although the intensities decrease. When the molar fraction of **4** increases up to 7.5%, 10% and 12.5%, the peak intensity of the (1 1 0) reflection further decreases and the diffraction peaks for the (2 0 0) and (3 1 1) reflections become less well resolved. Additionally, the (1 1 0) peak shifts toward higher angles with the increasing of the molar fraction of **4**, indicating that the dimensions of the unit cell gradually reduce. The increase in the molar fraction up to 15% leads to the nearly complete disappearance of these diffraction peaks, indicating a deterioration of the mesostructural ordering. The results can be explained by the fact that a higher amount of the bulky organosilane **4** led to a serious damage of the self-assembly by micelles (accompanied by a phase separation) and the part of amorphous silica thus dramatically increased.

TEM investigations show that the synthesized materials have highly ordered mesoporous structures similar to a typical SBA-16 till the molar fraction of **4** increases up to 10%. Fig. 1 selectively presents the TEM images for SBA-16-IPr(10%), SBA-16-IPr(12.5%)

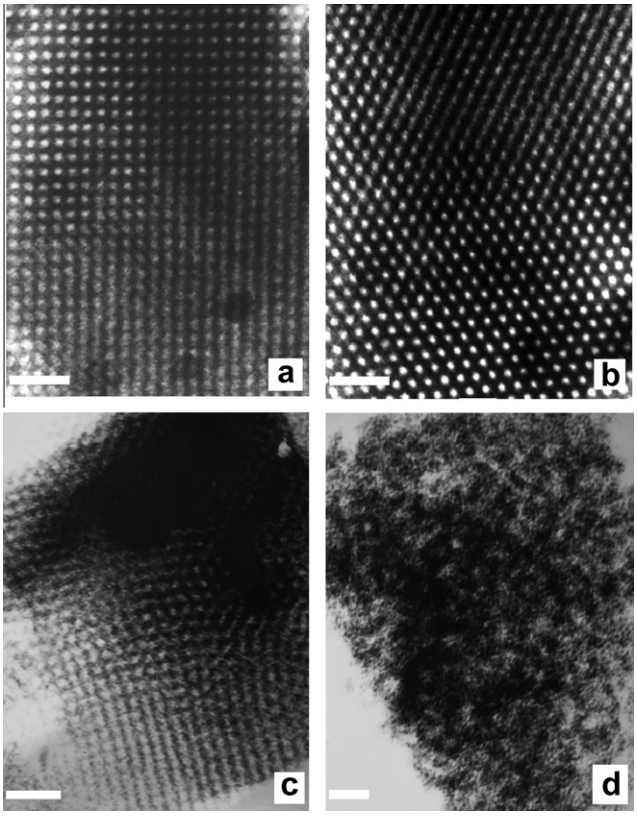

Fig. 1. TEM images for SBA-16-IPr(χ) materials. (a) SBA-16-IPr(10%); (b) SBA-16-IPr(10%); (c) SBA-16-IPr(12.5%); (d) SBA-16-IPr(15%). The bar is 50 nm.

and SBA-16-IPr(15%). In Fig. 1a and b, SBA-16-IPr(10%) clearly shows [1 0 0] and [1 1 1] projections of the cubic body-centered (*Im3m*) structure. When the molar fraction of **4** increases up to 12.5%, the regular arrays of pore ordering begin deforming (Fig. 1c). For SBA-16-IPr(15%) sample (Fig. 1d), the irregular pore arrays and nonuniform pore sizes are observed throughout the materials, which are consistent with XRD and N_2 sorption results.

Above N_2 sorption, XRD and TEM results reveal that an *Im3m* mesoporous structure can be achieved under the investigated conditions and that the amount of IPr precursor in the initial gel mixture has a significant effect on the mesoporous structure. The mesostructural ordering decreases as the amount of IPr precursor increases. Under the current synthesis conditions, 10 mol% is the up limit for achieving a good *Im3m* structure with a high specific surface area and pore volume.

3.3. Compositional characterization

To clarify the compositions of the synthesized materials, we employed FT-IR and solid-state NMR to further characterize the hybrid materials. Their FT-IR spectra are shown in Fig. 2. For comparison, the pure silica SBA-16 was synthesized. Its FT-IR spectrum is also included in Fig. 2. Compared with the FT-IR spectrum of pure silica SBA-16, the hybrid materials exhibit new peaks at 2976, 1542 and 1468 cm^{-1}. These three peaks correspond to C—H stretching, C=N stretching and C—H bending vibrations, suggesting that IPr precursor has been successfully incorporated into the solid materials. It is worthwhile to note that the intensities of such three peaks gradually increase as the molar fractions of **4** in the initial gel mixture increase. These results reflect that the amount of IPr precursor incorporated into the solid materials increases. The characteristic FT-IR signals (at *ca.* 1600 and

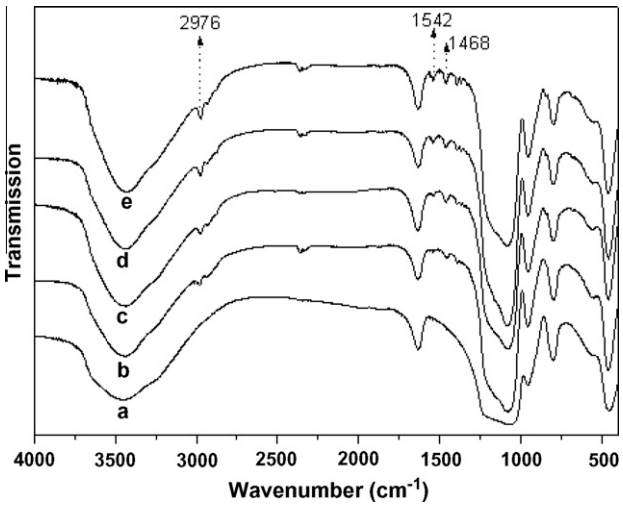

Fig. 2. FT-IR spectra for SBA-16-IPr(χ) materials. (a) SBA-16; (b) SBA-16-IPr(2.5%); (c) SBA-16-IPr(5%); (d) SBA-16-IPr(7.5%); (e) SBA-16-IPr(10%).

1350 cm^{-1}) for trifluoromethane sulfonate were not observed. It can be explained that trifluoromethane sulfonate was exchanged by Cl^- due to the presence of significantly excessive HCl under synthesis conditions. So, the eventual compositions of SBA-16-IPr(χ) materials are proposed as Scheme 2.

The quantitative determinations of **4** incorporated into the obtained materials were made with elemental analysis of C and N contents. The results are also included in Table 1. Elemental analysis revealed that the C and N contents gradually increased as the fraction of **4** in the initial gel mixture increased. The determined C contents for these four materials were higher with respect to the theoretical values calculated from the initial molar compositions, while the detected N contents were lower than their theoretical values. These results could be explained by the fact that a small amount of templates remained on the solid materials even after repeated solvent extractions due to the difficulty in the complete removal of templates for SBA-16 type of materials [43–45]. Based on the results of elemental analysis, it is estimated that *ca.* 4–6% templates of the initially added amount remained on the solid catalyst (on the assumption that alkoxy groups of **4** were completely condensed), namely the loading of the residue templates is *ca.* 3–5 μmol/g (F127). The comparison of the theoretical and the determined N contents reveals that *ca.* 86–100% of **4** in the initial gel

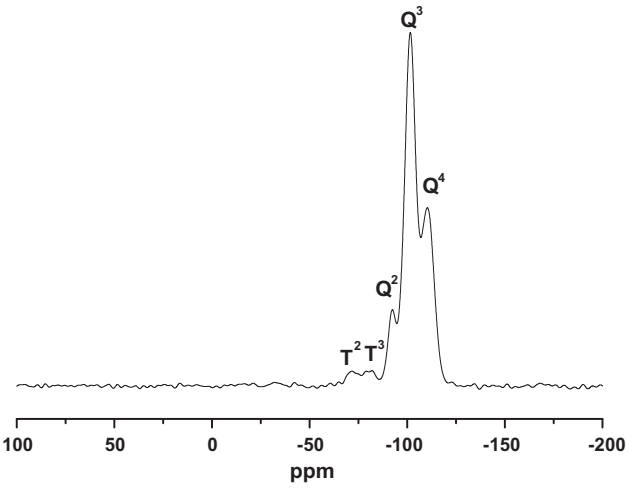

Fig. 3. ^{29}Si CP-MAS NMR spectrum for SBA-16-IPr(10%).

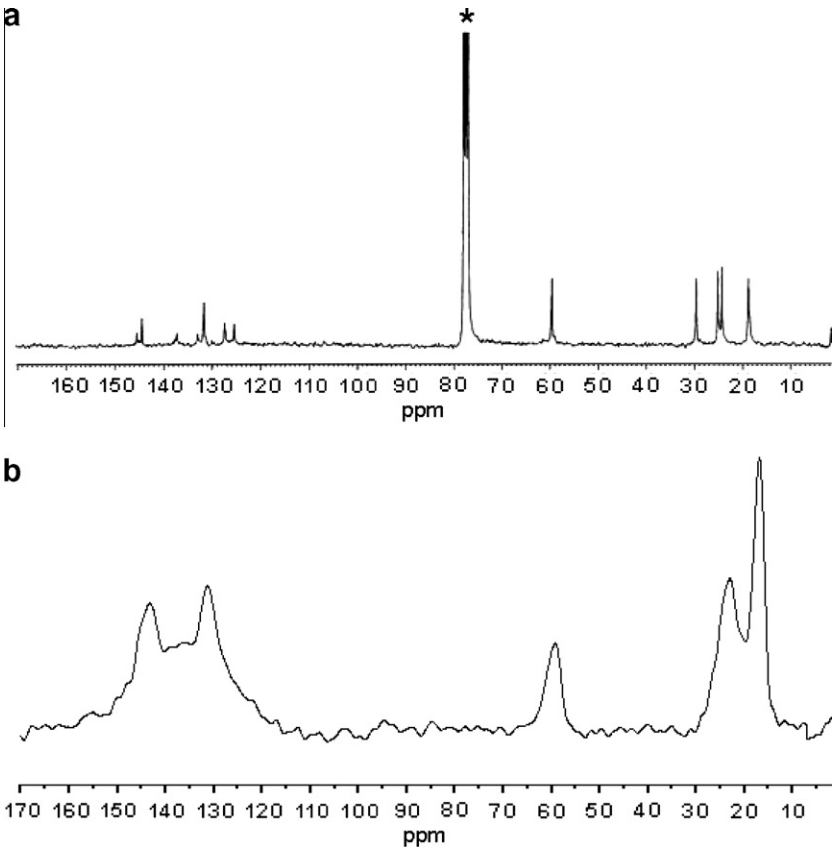

Fig. 4. ^{13}C NMR spectra. (A) ^{13}C NMR spectrum of **4**. (B) ^{13}C CP-MAS NMR spectrum for SBA-16-IPr(10%). Star peak is attributed to the solvent.

mixture was incorporated into the hybrid materials. Based on the determined N content, the IPr carbene precursor present on SBA-16-IPr(10%) is estimated to be 0.64 mmol/g.

Figs. 3 and 4 show the ^{29}Si CP-MAS NMR and ^{13}C CP-MAS NMR spectra of SBA-16-IPr(10%), respectively. In Fig. 3, the ^{29}Si CP-MAS NMR spectrum of SBA-16-IPr(10%) shows both "Q" and "T" silicon series. The signals at −110, −101 and −92 ppm correspond to Q^4 [$Si(OSi)_4$], Q^3 [$Si(OH)(OSi)_3$] and Q^2 [$Si(OH)_2(OSi)_2$] silicon sites, respectively. The peaks centered at −81 and −72 ppm are ascribed to T^3 [$SiC(OSi)_3$] and T_2 [$SiC(OH)(OSi)_2$] organosilicon sites, respectively. The presence of "T" bands indicates that IPr precursor has been incorporated in the framework through a Si—C linkage. For comparison, the liquid-state ^{13}C NMR spectrum of **4** and ^{13}C CP-MAS NMR spectra of SBA-16-IPr(10%) are displayed in Fig. 4. Similar to the liquid-state ^{13}C NMR spectrum (Fig. 4A), SBA-16-IPr(10%) clearly showed the signals for isopropyl groups on the aromatic rings at 24–30 ppm, and two aryl groups as well as the central imidazolium rings in the range 125–145 ppm (Fig. 4B). Their chemical shifts of liquid and solid sates are broadly in agreement with each other. The observed signal at 60 ppm indicates that a portion of $(EtO)_3Si$-groups were not completely hydrolyzed. It should be noted that the characteristic signals of template [at 71 ppm, —$(CH_2CH_2O)_n$—] were not observed. This is an indication that the content of the residual template is below the detection limit of solid-state NMR.

Above characterizations confirm that IPr precursor is covalently integrated with the hybrid materials.

3.4. Coordination of the hybrid materials with Pd(acac)$_2$

To probe the coordination capacity of IPr carbene in the solid framework, we chose Pd(acac)$_2$ (acac = acetylacetonate) to coordinate with the hybrid material because the formed Pd–IPr complex was stable in air and catalytically active for Suzuki–Miyaura reaction [9,46]. Pd(acac)$_2$ (2 wt%) with respect to SBA-16-IPr(10%) was used, which was sufficiently high for the catalytic reaction. The coordination was conducted in a 1,4-dioxane solution under the refluxing conditions. ICP-AES analysis revealed that the all Pd(acac)$_2$ in solution was loaded on the hybrid material under the investigated conditions. XPS spectroscopy was employed to investigate the coordination states of Pd species on the solid surface. Fig. 5 presents the XPS spectra of SBA-16-IPr(10%) derived with Pd(acac)$_2$ and pure Pd(acac)$_2$ complex. In Fig. 5A, XPS elemental survey scan of surface elementals of SBA-16-IPr(10%) derived with Pd(acac)$_2$ reveals that silicon, oxygen, carbon, nitrogen, palladium and chlorine elementals are present in the materials, as initially expected. In Fig. 5B, Pd(acac)$_2$ exhibits two peaks centered at 338.18 and 343.48 eV, which are assigned to Pd (II) $3d_{5/2}$ and Pd $3d_{3/2}$, respectively. Compared with the pure compound, the Pd $3d_{5/2}$ and $3d_{3/2}$ peaks for SBA-16-IPr(10%) derived with Pd(acac)$_2$ slightly shift down to 337.88 and 343.38 eV, respectively. Such changes may imply that new Pd(II) species were formed on the solid surface.

3.5. Suzuki–Miyaura reaction

To investigate the catalytic activities of the synthesized materials with different amounts of IPr, we coordinated SBA-16-IPr(χ) materials with 2 wt% Pd(acac)$_2$, yielding solid catalysts SBA-16-IPr(χ)–Pd. The pure silica SBA-16 was also derived with Pd(acac)$_2$ for comparison. Their catalytic activities were examined with Suzuki–Miyaura coupling of chlorobenzene and phenylboronic acid in *iso*-propyl alcohol at 80 °C under N_2 atmosphere. Potassium *tert*-butoxide was used as a base to promote this reaction [6,9]. The ratio of Pd to chlorobenzene was kept at 0.5 mol%. The reaction

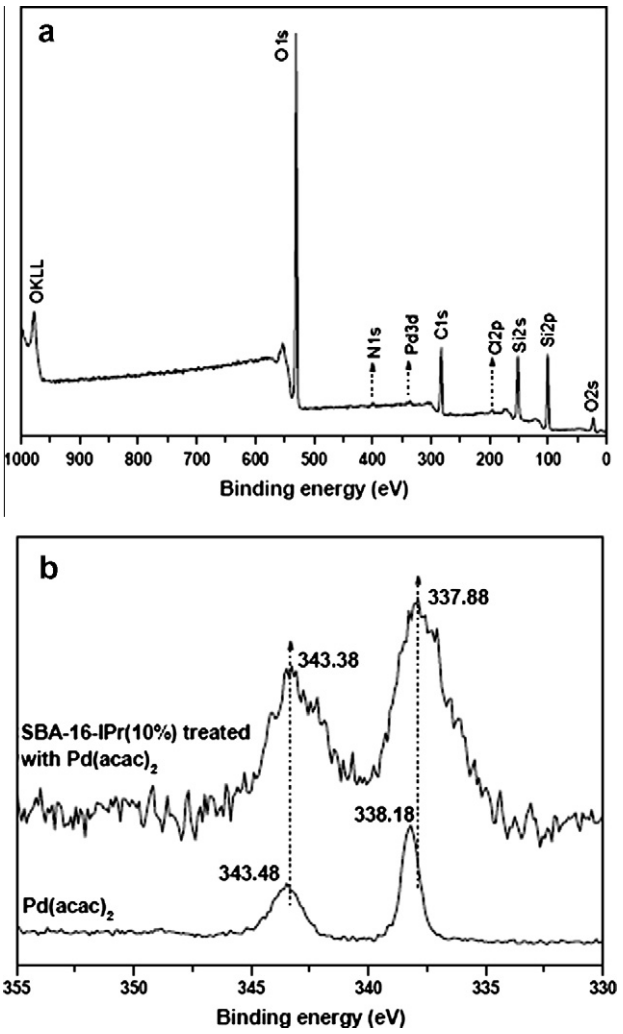

Fig. 5. XPS spectra of SBA-16-IPr(10%) derived with $Pd(acac)_2$. (A) The elemental survey scan of the material. (B) Pd XPS spectra of $Pd(acac)_2$ and SBA-16-IPr(10%) derived with $Pd(acac)_2$.

results are summarized in Table 2. Only a trace amount of product was detected for the pure silica SBA-16 derived with $Pd(acac)_2$ within 24 h. Under the same conditions, SBA-16-IPr(2.5%)–Pd afforded a 38% conversion. It is noteworthy that the increase in IPr contents leads to a continuous increase in the conversion. A conversion of 92% could be obtained on the catalyst SBA-16-IPr(10%)–Pd. The significantly improved conversions verified the role of IPr carbene in the framework in promoting the coupling reaction. However, the IPr contents in framework further increased, and the conversion was observed to decrease. For SBA-16-IPr(15%)–Pd, the conversion decreased down to 79%. The decreased activity is probably due to the reduced surface area of the hybrid material. These primary investigations showed that the activity of the hybrid solid catalyst was dependent on not only the IPr content of the solid material but also the structure of the solid material. SBA-16-IPr(10%)–Pd exhibits the highest activity among the investigated solid catalysts. On this occasion, the ratio of IPr/Pd is estimated to be 9.8. The decrease in the ratio of IPr/Pd led to a slight reduction in conversion (the ratio of 6.5 gave a 90% conversion under the same conditions). In view of the stability of the heterogeneous catalysts, the excessive IPr precursors may be also desired because the uncoordinated IPr precursors in the framework as ionic liquids help to stabilize the *in situ*-formed Pd(0) nanoparticles against growth [18].

Suzuki–Miyaura couplings of other aryl halides and phenylboronic acid were also examined. The corresponding results are included in Table 3. SBA-16-IPr(10%)–Pd was catalytically active toward all the substrates examined. This solid catalyst gave biphenyl in an isolated yield of 78% at 80 °C within 24 h (Table 3, entry 1, Fig.S4 of Supplementary material). Under the same conditions, its counterpart [treating **4** with $Pd(acac)_2$] gave an 80% yield within 8 h. The decreased activity of the complex after immobilization may be partially due to the diffusion limitations inside the nanopores. For aryl chloride bearing an electron-withdrawing group, an 89% yield was obtained in a shorter reaction time and the lower Pd loading led to a relatively lower conversion (Table 3, entry 2). This catalyst could afford good yields for aryl chlorides bearing electron-denoting groups such as $-CH_3$ and $-OCH_3$ (Table 3, entries 3 and 4). To our delight, for electron-rich aryl chlorides with steric hindrances such as 2-methylchlorobenzene and 2,4-dimethylchlorobenzene, moderate to good yields could also be achieved (Table 3, entries 5 and 6). Additionally, aryl bromides could be easily converted to the corresponding products in excellent yields over this solid catalyst (Table 3, entries 7 and 8).

We further tested its catalytic activities for the coupling of various arylboronic acids with chlorobenzene. These results are summarized in Table 4. For electron-rich arylboronic acids, SBA-16-IPr(10%)–Pd gave good yields (Table 4, entries 1 and 2). For electron-rich arylboronic acids with moderate steric hindrances, moderate to good yields were obtained (Table 4, entries 3 and 4). The relatively lower yield was achieved for electron-poor arylboronic acid (Table 4, entry 5). The differences in yields reflect the electron effects on the activity of the solid catalyst. The above activity tests suggest that the developed catalyst can represent one of the most efficient solid catalysts for Suzuki–Miyaura coupling of the challenging aryl chlorides under relatively mild conditions, although its preparation procedure is more complex than those of the previously reported catalysts such as Pd/C catalyst [15,16,47–50]. The outstanding activity toward aryl chlorides may be attributed to the strong σ-donor ligand (IPr carbene) in the framework and the open structure of the solid catalyst. The strong σ-donor ligand is necessary to reach a high degree of efficiency, and the open structure is helpful for the access of the substrates.

The recyclability of SBA-16-IPr(10%)–Pd was investigated with the consecutive Suzuki–Miyaura couplings of 4′-chloroacetophe-

Table 2
Suzuki–Miyaura coupling reactions catalyzed by SBA-16-IPr(χ) materials derived with $Pd(acac)_2$.

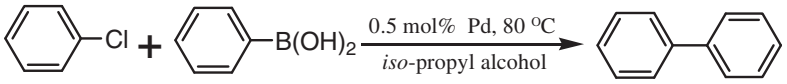

Samples	SBA-16	SBA-16-IPr(2.5%)	SBA-16-IPr(5%)	SBA-16-IPr(7.5%)	SBA-16-IPr(10%)	SBA-16-IPr(12.5%)	SBA-16-IPr(15%)
Conv.[a] (%)	<1	38	72	79	92	89	79

[a] The conversions were determined with GC.

Table 3
Suzuki–Miyaura couplings of various aryl halides and phenylboronic acid over SBA-16-IPr(10%)–Pd.

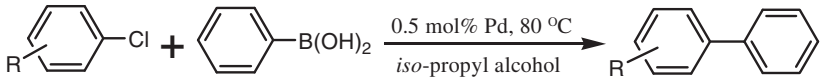

Entry	Substrate	Product	Pd (mol%)	Time (h)	Yield[a] (%)
1	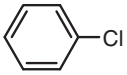	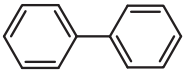	0.5	24	78
2	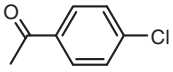	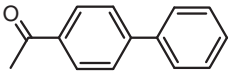	0.5 (0.1)	20 (20)	89 (69)
3	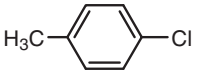	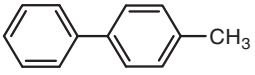	0.5	24	71
4	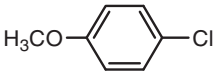	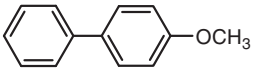	0.5	24	68
5	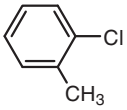	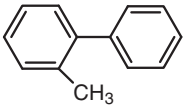	0.5	24	70
6	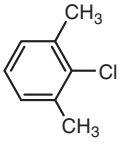	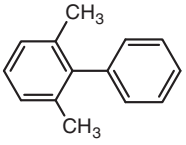	0.5	24	50[b]
7	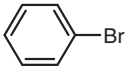	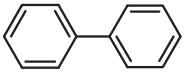	0.25	6	90
8	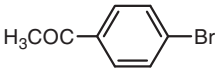		0.25	6	92

[a] The isolated yield.
[b] Determined with GC.

Table 4
Suzuki–Miyaura couplings of various phenylboronic acids and chlorobenzene over SBA-16-IPr(10%)–Pd.

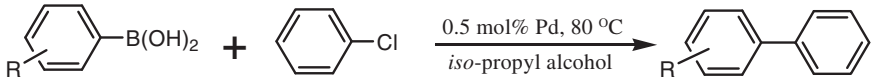

Entry	Substrate	Product	Yield[a] (%)
1	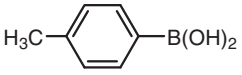	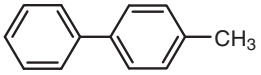	85
2	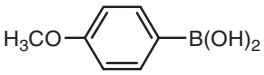	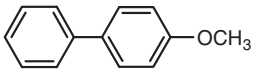	77
3	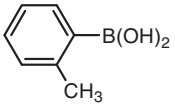	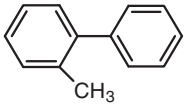	72
4	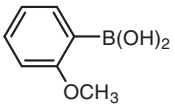	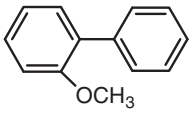	49
5	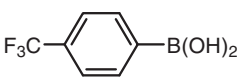	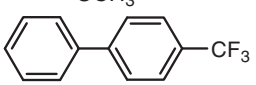	66

[a] Isolated yields.

none with phenylboronic acid. Due to the unavoidable loss of solid catalyst during the course of recovery and washing, the reaction scale was amplified six times to ensure that the catalyst of good quality was available for us to perform the several consecutive recycling reactions, as described in Experimental. The recycling results of SBA-16-IPr(10%)–Pd are summarized in Table 5. Under the scale-up conditions, the fresh solid gave the product in an 89% yield within 20 h. After the first reaction cycle, the catalyst could be recovered by centrifugation along with filtration. After being washed and dried, the recovered catalyst was directly used for the next reaction cycle. From the second to the fourth reaction cycle, the 85–89% yields of acetylbiphenyl were achieved without a prolonged time. Beginning with the fifth reaction cycle, a slight longer reaction time was needed to complete the reaction, and 81–87% yields were obtained from the fifth to the seventh reaction cycle. For the eighth reaction cycle, an 84% yield was still attained. Although the activity of the solid catalyst slightly decreases during recycling, it represents one of the most robust heterogeneous catalysts for Suzuki–Miyaura coupling of aryl chlorides [15,16,47–49]. After the coupling reaction of chlorobenzene with phenylboronic

Table 5
Recyclability test of SBA-16-IPr(10%)–Pd with the Suzuki–Miyaura coupling reaction.

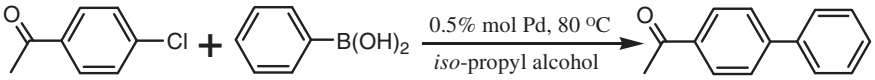

Cycles	1	2	3	4	5	6	7	8
Time (h)	20	20	20	20	24	26	28	34
Yield[a] (%)	89	88	85	89	87	81	83	84

[a] Isolated yield.

Table 6
The coupling reactions of benzylic/allylic chlorides and arylboronic acids over SBA-16-IPr(10%)–Pd.[a]

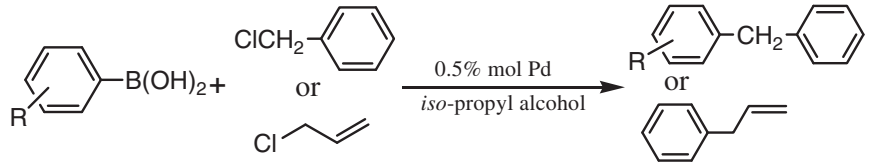

Entry	Arylboronic acids	Products	Time (h)	Yield[b] (%)
1	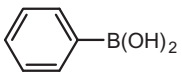	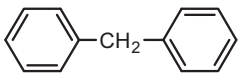	10	88
2	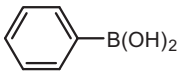	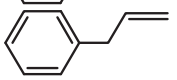	12	71
3	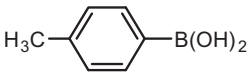	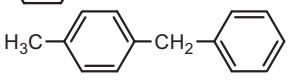	10	90
4	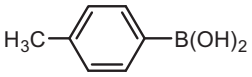	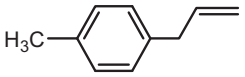	12	68
5	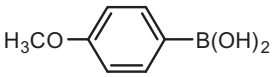	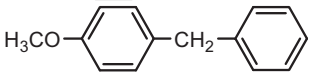	10	92
6	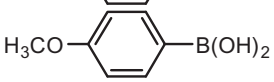	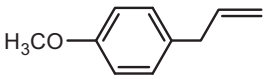	12	61
7	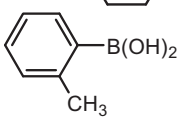	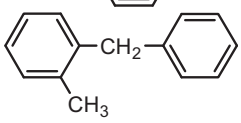	10	91
8	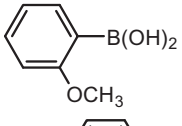	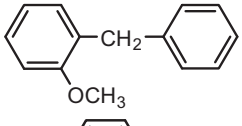	10	95
9	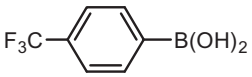	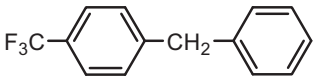	10	89

[a] For benzylic chloride, the reaction temperature was 80 °C; for allylic chloride, the reaction temperature was 50 °C.
[b] Isolated yield.

acid proceeded for 6 h (the conversion at 50%), the reaction was stopped and the filtrate was immediately collected under the hot conditions. A further 4% increase in conversion was observed after heating the filtrate at 80 °C for another 18 h (50% of the initial *t*-BuOK amount was added to the filtrate). These results may indicate that the observed conversion was at least partially contributed by the leached Pd species in the filtrate. Interestingly, the determination of the Pd content on the catalyst used once reveals that *ca*. 98% Pd of the fresh catalyst was kept on the recovered solid catalyst. The TEM image reveals that the mesoporous structure of the recovered catalyst roughly survived the first reaction cycle and that Pd nanoparticles are present on the solid catalyst used once as the homogeneous system (Figs.S5 and S6 in Supplementary material). Clearly, the Pd particles' sizes for the homogeneous system are not uniform. Some of them are larger than those for the heterogeneous system. The above investigations demonstrate the role of the solid material in the Pd recovery and stabilizing the Pd nanoparticles. Additionally, the hybrid solid catalyst exhibited high stability in air. It was found that there was not decrease in activity after the catalyst was exposed to air for one month.

3.6. The coupling reactions of benzylic/allylic chlorides and arylboronic acid

Encouraged by the impressive results for Suzuki–Miyaura couplings of aryl chlorides and boronic acid, we wanted to test the catalytic activity toward the couplings of benzylic/allylic chlorides and arylboronic acids. This coupling reaction provides an important alternative to the Friedel–Crafts reaction for the synthesis of diarylmethane and allylic aromatics [51–53]. However, to our knowledge, few heterogeneous catalysts have been reported. The results for benzylic chloride couplings and allylic chloride couplings are summarized in Table 6. Using phenylboronic acid as a substrate, the solid catalyst SBA-16-IPr(10%)–Pd afforded diphenylmethane in a yield up to 88% and allylbenzene in a 71% yield (Table 6, entries 1 and 2). In followed reactions, in spite of electron-rich arylboronic acids (Table 6, entries 3, 5, 7 and 8) and electron-poor arylboronic acid (Table 6, entry 9), various diarylmethane-type compounds in 89–90% yields were obtained. In the cases of allylic chlorides, allylic compounds in moderate to good yields were also achieved (Table 6, entries 4 and 6).

4. Conclusions

We have successfully synthesized new 3D cage-like mesoporous materials containing a well-known NHC ligand (IPr) precursor in the framework by co-condensation of IPr precursor-bridged triethoxysilane and TEOS in the presence of template. The mesostructure and textural properties of the obtained hybrid materials depended on the amount of the bridged organosilane introduced into the initial gel mixture. A well-ordered 3D mesostructure could be achieved when the IPr loading on the solid material was lower than 0.64 mmol/g. Such hybrid materials were able to coordinate $Pd(acac)_2$, leading to active solid catalysts for Suzuki–Miyaura couplings of electron-rich aryl chlorides even with steric hindrances. Their catalytic activities were related to the IPr contents and the structural properties of the hybrid materials. This solid catalyst could be reused 8 times without a significant decrease in activity. Furthermore, the solid catalysts were active toward the couplings of $C(sp^3)$-chlorides and arylboronic acids. This study supplies a new 3D mesoporous hybrid material with a versatile IPr carbene integrated in the solid framework, which is applicable to other catalytic reactions such as aryl amination [5], cycloaddition [54], transesterification [55] and cyclotrimerization of isocyanates [56].

Acknowledgments

We acknowledge New Teacher Foundation from Education Ministry of China (200801081035), Shanxi Natural Science Foundation for Youths (2009021009), the Natural Science Foundation of China (NSF20903064), Shanxi University Innovative Experimental Project for Undergraduates and Jiangsu Key Lab. of Fine Petrochemistry for financial supports (KF0802). We also thank Dr. Lei Zhang (BASF, Nederland, BV, De Meern) for his help with this manuscript.

Appendix A. Supplementary material

Supplementary data associated with this article can be found, in the online version, at doi:10.1016/j.jcat.2010.09.004.

References

[1] N. Miyaura, T. Yanagi, A. Suzuki, Synth. Commun. 11 (1981) 513.
[2] L. Yin, J. Liebscher, Chem. Rev. 107 (2007) 133.
[3] J.S. Carey, D. Laffan, C. Thomsonc, M.T. Williamsd, Org. Biomol. Chem. 4 (2006) 2337.
[4] E.A.B. Kantchev, C.J. O'Brien, M.G. Organ, Angew. Chem. Int. Ed. 46 (2007) 2768.
[5] M.G. Organ, M. Abdel-Hadi, S. Avola, I. Dubovyk, N. Hadei, E.A.B. Kantchev, C.J. O'Brien, M. Sayah, C. Valente, Chem. Eur. J. 14 (2008) 2443.
[6] N. Marion, E.C. Ecarnot, O. Navarro, D. Amoroso, A. Bell, S.P. Nolan, J. Org. Chem. 71 (2006) 3816.
[7] N. Marion, O. Navarro, J. Mei, E.D. Stevens, N.M. Scott, S.P. Nolan, J. Am. Chem. Soc. 128 (2006) 4101.
[8] O. Diebolt, P. Braunstein, S.P. Nolan, C.S.J. Cazin, Chem. Commun. (2008) 3190.
[9] N. Marion, P.D. Frémont, I.M. Puijk, E.C. Ecarnot, Adv. Synth. Catal. 349 (2007) 2380.
[10] G.R. Peh, E.A.B. Kantchev, J.C. Er, J.Y. Ying, Chem. Eur. J. 16 (2010) 4010.
[11] T.K. Maishal, J. Alauzun, J.M. Basset, C. Copéret, R.J.P. Corriu, E. Jeanneau, A. Mehdi, C. Reyé, L. Veyre, C. Thieuleux, Angew. Chem. Int. Ed. 47 (2008) 8654.
[12] I. Karam, M. Boualleg, J.M. Camus, T.K. Maishal, J. Alauzun, J.M. Basset, C. Copéret, R.J.P. Corriu, E. Jeanneau, A. Mehdi, C. Reyé, L. Veyre, C. Thieuleux, Chem. Eur. J. 15 (2009) 11820.
[13] P. Han, H.M. Zhang, X.P. Qiu, X.L. Ji, L.X. Gao, J. Mol. Catal. A: Chem. 295 (2008) 57.
[14] V. Polshettiwar, P. Hesemann, J.J.E. Moreau, Tetrahed. Lett. 48 (2007) 5363.
[15] J.H. Kim, J.W. Kim, M. Shokouhimehr, Y.S. Lee, J. Org. Chem. 70 (2005) 6714.
[16] D.H. Lee, J.H. Kim, B.H. Jun, H. Kang, J. Park, Y.S. Lee, Org. Lett. 10 (2008) 1609.
[17] H. Hagiwara, K.H. Ko, T. Hoshi, T. Suzuki, Chem. Commun. (2007) 2838.
[18] H.Q. Yang, X.J. Han, G. Li, Y.W. Wang, Green Chem. 11 (2009) 1184.
[19] J.W. Byun, Y.S. Lee, Tetrahed. Lett. 45 (2004) 1837.
[20] Q.H. Yang, J. Liu, L. Zhang, C. Li, J. Mater. Chem. 19 (2009) 1945.
[21] S. Inagaki, S. Guan, Y. Fukushima, T. Ohsuna, O. Terasaki, J. Am. Chem. Soc. 12 (1999) 9611.
[22] B.J. Melde, B.T. Holland, C.F. Blanford, A. Stein, Chem. Mater. 11 (1999) 3302.
[23] T. Asefa, M.J. MacLachlan, N. Coombs, G.A. Ozin, Nature 402 (1999) 867.
[24] L. Zhang, J. Liu, J. Yang, Q.H. Yang, C. Li, Chem. Asian J. 3 (2008) 1842.
[25] D.M. Jiang, Q.H. Yang, H. Wang, G.R. Zhu, J. Yang, C. Li, J. Catal. 239 (2006) 65.
[26] D.A. Loyt, K.J. Shea, Chem. Rev. 95 (1995) 1431.
[27] Y. Wan, D.Q. Zhang, Y.P. Zhai, C.M. Feng, J. Chen, H.X. Li, Chem. Asian J. 2 (2007) 875.
[28] H.Q. Yang, G.Y. Zhang, X.L. Hong, Y.Y. Zhu, J. Mol. Catal. A: Chem. 210 (2004) 143.
[29] A. Corma, D. Das, H. García, A. Leyva, J. Catal. 229 (2005) 322.
[30] V. Dufaud, F. Beauchesne, L. Bonneviot, Angew. Chem. Int. Ed. 44 (2005) 3475.
[31] C. Baleizão, B. Gigante, D. Das, M. Vlvaro, H. García, A. Corma, J. Catal. 223 (2004) 106.
[32] P.Y. Wang, X. Liu, J. Yang, Y. Yang, L. Zhang, Q.H. Yang, C. Li, J. Mater. Chem. 19 (2009) 8009.
[33] E.B. Cho, D. Kim, J. Gorka, M. Jaroniec, J. Mater. Chem. 19 (2009) 2076.
[34] P. Nguyen, P. Hesemann, P. Gaveau, J.J.E. Moreau, J. Mater. Chem. 19 (2009) 4164.
[35] H. Skaff, T. Emrick, Chem. Commun. (2003) 52.
[36] T.W. Kim, R. Ryoo, M. Kruk, K.P. Gierszal, M. Jaroniec, S. Kamiya, O. Terasaki, J. Phys. Chem. B 108 (2004) 11480.
[37] O.C. Gobin, Y. Wan, D.Y. Zhao, F. Kleitz, S. Kaliaguine, J. Phys. Chem. C 111 (2007) 3053.
[38] H.Q. Yang, J. Li, J. Yang, Z.M. Liu, Q.H. Yang, C. Li, Chem. Commun. (2007) 1086.
[39] D. Zhao, Q. Huo, J. Feng, B.F. Chmelka, G.D. Stucky, J. Am. Chem. Soc. 120 (1998) 6024.
[40] Y. Sakamoto, M. Kaneda, O. Terasaki, D. Zhao, J.M. Kim, G.D. Stucky, H.J. Shin, R. Ryoo, Nature 408 (2000) 449.
[41] R.M. Grudzien, S. Pikus, M. Jaroniec, J. Phys. Chem. B 110 (2006) 2972.
[42] J. Liu, Q.H. Yang, L. Zhang, D.M. Jiang, X. Shi, J. Yang, H. Zhong, C. Li, Adv. Funct. Mater. 17 (2007) 569.
[43] R.M. Grudzien, J.P. Blitz, S. Pikus, M. Jaroniec, Micropor. Mesopor. Mater. 118 (2009) 68.

[44] R.M. Grudzien, B.E. Grabicka, M. Jaroniec, J. Mater. Chem. 16 (2006) 819.
[45] A. Boullanger, J. Alauzun, A. Mehdi, C. Reyé, R.J.P. Corriu, New J. Chem. 34 (2010) 738.
[46] O.H. Winkelmann, A. Riekstins, S.P. Nolan, O. Navarro, Organometallics 28 (2009) 5809.
[47] M. Trilla, G. Borja, R. Pleixats, M.W.C. Man, C. Bied, J.J.E. Moreau, Adv. Synth. Catal. 350 (2008) 2566.
[48] K. Glegoła, E. Framery, K.M. Pietrusiewicz, D. Sinou, Adv. Synth. Catal. 348 (2006) 1728.
[49] M.J. Jin, D.H. Lee, Angew. Chem. Int. Ed. 49 (2010) 1119.
[50] C.R. LeBlond, A.T. Andrews, Y. Sun, J.R. Sowa Jr., Org. Lett. 3 (2001) 1555.
[51] M.J. Burns, I.J.S. Fairlamb, A.R. Kapdi, P. Sehnal, R.J.K. Taylor, Org. Lett. 9 (2007) 5397.
[52] B.P. Bandgar, S.V. Bettigeri, J. Phopase, Tetrahed. Lett. 45 (2004) 6959.
[53] R. Singh, M.S. Viciu, N. Kramareva, O. Navarro, S.P. Nolan, Org. Lett. 7 (2005) 1829.
[54] S. Díez-González, E.D. Stevens, S.P. Nolan, Chem. Commun. (2008) 4747.
[55] G.A. Grasa, T. Gveli, R. Singh, S.P. Nolan, J. Org. Chem. 68 (2003) 2812.
[56] H.A. Duong, M.J. Cross, J. Louie, Org. Lett. 6 (2004) 4679.